AIChE WILEY InterScience DISCOVER SOMETHING GREAT

PARTICLE TECHNOLOGY AND FLUIDIZATION

Design of Granule Structure: Computational Methods and Experimental Realization

Mansoor A. Ansari and Frantisek Stepanek
Dept. of Chemical Engineering, Imperial College London, South Kensington campus, London SW7 2AZ, U.K.

DOI 10.1002/aic.10990
Published online September 13, 2006 in Wiley InterScience (www.interscience.wiley.com).

The spatial distribution of solid components and porosity within a composite granule—its microstructure—is an important attribute as it carries information about the processing history of the granule and determines its end-use application properties, particularly the dissolution rate. In this work, the problem of rational design of granule structure is formulated, and two methods for its solution are proposed—stochastic design, which is based on random permutation of points within the structure using the simulated annealing algorithm, and variational design, which is based on direct simulation of granule formation from its constituent primary particles, followed by direct simulation of granule dissolution. The variational design method is demonstrated in a case study of the effect of primary particle size, radial distribution of components, and composition of a two-component granule (active, excipient) on the dissolution profile. Selected granule structures designed computationally were also physically made by fluid-bed granulation, their structure analyzed by X-ray micro-tomography, and dissolution curves measured. It was confirmed that the designed structures are feasible to manufacture and that they meet the required dissolution profiles. © 2006 American Institute of Chemical Engineers *AIChE J,* 52: 3762–3774, 2006

Keywords: granulation, dissolution, microstructure, product design, mathematical modeling

Introduction

Granules—that is, agglomerates of primary solid particles—represent an important class of products manufactured by the chemical process industries. Examples of product categories supplied in the form of granules include fertilizers, foods, detergents, and pharmaceuticals.[1] In these formulated products, the granule typically contains one or more main functional ingredients as well as a number of other, auxiliary formulation components. From the application point of view, the granule can be regarded as a delivery form because most of the active ingredients eventually perform their function in solution.[2] The rate at which the active ingredients are released from the granule into a solution during end-use application depends on the physico-chemical properties of all the components (their individual solubility and diffusion coefficient) and on the granule *microstructure*—that is, on the spatial distribution of the formulation components and porosity within the granule.

The physico-chemical properties of the ingredients are given by their molecular composition. Therefore, once the formulation (the ingredient list) is fixed during the initial "chemical" phase of product development, modification of the granule microstructure during the "engineering" phase of product development remains as the only possibility to control the dissolution rate of the final product. The microstructure is the result of four factors: (*i*) the process by which the granule has been formed (high-shear granulation, fluid-bed granulation, and so forth), (*ii*) the initial physical state of the formulation ingredients (initial particle size, and so forth), (*iii*) the order of their addition into the granulation process, and (*iv*) the specific granulation process conditions (shear rate, temperature, binder spray-on rate, and so forth). Microstructure is, therefore, an

Correspondence concerning this article should be addressed to F. Stepanek at f.stepanek@imperial.ac.uk.

© 2006 American Institute of Chemical Engineers

important attribute that, on the one hand, carries information about the processing history, and on the other hand, co-determines the end-use application performance of a formulated product.

Despite the stated importance of microstructure, very few studies linking granule microstructure quantitatively to processing conditions and end-use behavior (dissolution) can be found in the literature.[3] Perhaps as a consequence, granule microstructure per se is not normally specified as a target attribute during product development, that is, it is not the focus of systematic and rational design activity in the same sense as the product composition (formulation) normally is.[4,5] Instead, the common practice during the engineering phase of product development is to engage in a more-or-less empirical search for a combination of granulation process parameters that result into granules with satisfactory dissolution profiles,[6] without necessarily knowing which features of the granule microstructure are being modified and to what extent. This leads to inefficiency in the product development process and, ultimately, longer time-to-market.

The objective of our present work, therefore, is to help establish quantitative relationships between processing, microstructure, and end-use behavior (dissolution) through a combination of physical experiments and computer simulation studies, and to develop a systematic procedure for rational granule microstructure design. This article is organized as follows: First, the microstructure design problem is posed in a mathematically rigorous way and two different approaches to its solution, called stochastic and variational, are proposed. The latter approach is then demonstrated in a case study involving the design of a two-component granule with a specified release profile of one of the components. Experimental granulation protocols for the preparation of the proposed designs are then shown, the granule microstructures analyzed by X-ray microtomography, and the dissolution curves of the prepared granules are measured and compared with those predicted by computer simulations. Finally, conclusions are drawn and directions for future research indicated.

The Microstructure Design Problem

Problem formulation

Let us consider the following problem: It is required to produce a granule with radius R that must be between $R_{min} \leq R \leq R_{max}$ and composition specified by a vector of K mass fractions of the formulation ingredients, $\mathbf{w} = [w_1, w_2, \ldots, w_K]$, such that a specified release rate of one of the components (further called the "active") from the granule be met. Let the requirement on the release rate be given in the form of integral characteristics such as the t_{10}, t_{50}, and t_{90} (the time necessary for 10, 50, and 90%, respectively, of the active to be released into the solution under specified temperature and hydrodynamic conditions). The unknown in this problem is the granule radius R and a set of $K + 1$ phase functions, $f_k(\mathbf{r})$, that describe the spatial distribution of each formulation ingredient and porosity within the granule—that is, they uniquely define the microstructure. The phase functions[7] are defined as:

$$f_k(\mathbf{r}) = \begin{cases} 1 & \text{if point } \mathbf{r} \text{ contains component } k \\ 0 & \text{otherwise} \end{cases} \quad (1)$$

and it is further required that $\sum_{k=1}^{K+1} f_k(\mathbf{r}) = 1$ in every point $\mathbf{r}$. The structure of the granule is normally encoded on a discrete three-dimensional grid of $N_x \times N_y \times N_z$ volume elements (voxels) with spatial step (resolution) h. Each "point" $\mathbf{r}$ in that case denotes the coordinates of a single voxel on this discrete grid, rather than a true point in the continuous real space $\Re^3$.

Depending on the physico-chemical properties of the formulation components (their individual dissolution rates), there may be no structure that satisfies the problem specification, there can be a finite number of such structures, or a continuum of possible solutions. In the former case, the product must be reformulated or some of the requirements on size or dissolution profile relaxed. In the latter cases, the remaining degrees of freedom give the opportunity to impose further constraints, pose an optimization problem, or simply choose a structure that is the most "simple" to make in some sense (for example, requiring little or no customization of existing process setup).

Let Ω be a set of solutions of the granule design problem, that is, a set of all microstructures (phase functions) that satisfy the requirement on dissolution profile and granule composition. Let us also define $\Omega_F \subset \Omega$ to be a set of *feasible* microstructures, that is, such microstructures that can be formed by conventional granulation processes or their combination. On the other hand, microstructures belonging to $\Omega_H = \Omega - \Omega_F$ will be called *hypothetical* microstructures. Although such microstructures satisfy the requirement on dissolution time, the spatial arrangement of the K components and porosity in these structures is such that it cannot be physically realized by existing (conventional) granulation processes. Although one is primarily interested in identifying microstructures belonging to Ω_F, those from Ω_H are also interesting—not only from the theoretical point of view but also practically. If a hypothetical microstructure gives a significantly improved end-use performance compared with any existing one, this may be an incentive for the development of novel granulation processes. On the other hand, if even the "best" hypothetical microstructure is only marginally better than any of the feasible ones, this means that no significant opportunities for product improvement are being missed. Let us now describe two solution strategies to the design problem posed above.

Stochastic design method

The stochastic design procedure starts from a random distribution of components in the granule structure, that is, random initial phase functions $f_k(\mathbf{r})$, which are iteratively updated according to the Metropolis algorithm.[8] In every iteration step, two points within the granule, $\mathbf{r}_1$ and $\mathbf{r}_2$, are randomly chosen and their phase functions swapped. The dissolution profile of the new microstructure is then calculated by means of the dissolution model described in the section "Granule dissolution model" below. Formally, the action of the dissolution model can be represented as a mapping, D, from the microstructure space to the space of dissolution profiles, that is, $[t_{10},t_{50},t_{90}] = D(f_k)$, as shown schematically in Figure 1. The root mean square error is evaluated as a measure of the difference between the required (t^*) and calculated (t^i in the i-th iteration step) dissolution time:

$$o^i = \sqrt{\frac{(t^i_{10} - t^*_{10})^2 + (t^i_{50} - t^*_{50})^2 + (t^i_{90} - t^*_{90})^2}{3}} \quad (2)$$

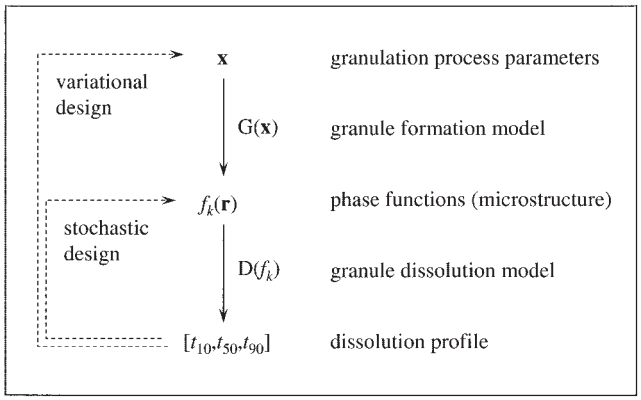

Figure 1. Representation of the functional relationship between granulation process parameters, *x*, the granule microstructure, f_k, the dissolution profile, $[t_{10},t_{50},t_{90}]$, and the stochastic and variational approaches to granule structure design.

If $o^i \leq o^{i-1}$ (that is, if the dissolution profile in the i-th iteration is closer to the required one than in the previous iteration), the new microstructure is accepted. On the other hand, if $o^i > o^{i-1}$, the swap of phase functions between the two points is only accepted with a probability

$$p = \exp\left(\frac{o^{i-1} - o^i}{T}\right). \tag{3}$$

Here, T is a fictitious temperature, which may change in the course of iteration in order to improve convergence (simulated annealing). The algorithm ends when no significant improvement in o^i occurs over a specified number of successive iterations.

The main attraction of the stochastic approach is that it can lead to the "discovery" of entirely new, unexpected microstructures. The main disadvantages are that the majority of microstructures obtained by stochastic design tend to belong to Ω_H and that no information about how to physically make these structures is provided. The use of the stochastic approach to granule design is described in a separate article.[9] Beyond granulation, the stochastic approach has been applied, for example, for the reconstruction of porous media having specified two-point correlation function.[10] Also the problem of designing composite materials with a required thermal and electric conductivity has been solved by a similar method.[11,12]

Variational design method

The variational design of granule microstructure is based on a rather different philosophy: New granule microstructures are not generated by random permutations of points within the microstructure itself, but constructed by the simulation of the process of granule formation from its constituent parts (primary particles) according to a granulation model described in the section "Granule formation model" below. The granule formation model can be formally represented by a mapping, G, from the space of the granulation process parameters to the space of phase functions (microstructures), that is, $[f_1(\mathbf{r}),f_2(\mathbf{r}),\ldots f_{K+1}(\mathbf{r})] = G(\mathbf{x})$, as shown in Figure 1. Parameters that control the granule structure formation for a fixed composition are the primary particle sizes, the sequence of primary particle addition, and in the case of wet granulation, also the binder droplet size and the binder solidification rate. These parameters are systematically varied (hence, the name variational) until a structure is generated whose dissolution profile closely matches the required one.

Finding such microstructure in a rigorous way involves solving an optimization problem to minimize o (defined by Eq. 2) with respect to $\mathbf{x}$, where $\mathbf{x}$ is a vector of N input parameters for the granule microstructure formation model. The main factor affecting the choice of the optimization method is that a single evaluation of the objective function $o(\mathbf{x})$ involves the simulation of granule formation, $G(\mathbf{x})$, and dissolution, $D(f_k)$, both of which are relatively time-consuming. Gradient-based methods, such as the steepest-descent method, requiring numerical evaluation of partial derivatives in $\mathbf{g} = [(\partial o/\partial x_1) \cdots (\partial o/\partial x_N)]^T$, would, therefore, be computationally prohibitive. Direct-search methods such as interval halving or the Nelder-Mead algorithm tend to be more appropriate for situations where the objective function does not exist in closed form.[13] In this work, we construct the dependence of the dissolution profile on individual granulation parameters (particle size, order of addition, pure component dissolution rates) by a parametric study (see the section "Structure-dissolution relationships"). This can be regarded as a grid-based direct-search method—that is, the objective function is directly evaluated for a priori selected values of the independent variable $\mathbf{x}$ in order to gain information about its shape. The heuristics generated in this way can then be used for actual design.

An advantage of the variational approach is that by linking granulation process parameters to the dissolution profile via granule microstructure (see Figure 1), it is in fact a computational analogy of physical experiments. Therefore, once a solution to the optimization problem, $\mathbf{x}^*$, is found, it can be used directly to guide the physical preparation of a small batch of the proposed granule design. The second major advantage of the variational design approach is that by definition it generates only feasible structures (Ω_F). A disadvantage of the variational design approach is that there is always a possibility of missing potentially superior microstructures if the initial estimates $\mathbf{x}^0$ are chosen outside their domains of attraction in the parameter space.

Auxiliary models

Both methods for the solution of the granule design problem require a granule dissolution model in order to calculate the dissolution profile from a given microstructure and, hence, the error, o. The variational method also requires a model of granule formation.

Granule Dissolution Model. The granule dissolution model is based on our earlier work.[14] The input to the model is the granule structure encoded by the phase functions, $f_k(\mathbf{r})$, and the density ρ_k, solubility c_k^*, and diffusion coefficient in water D_k (at a given temperature) of each component. The granule dissolution profile is obtained by the solution of the diffusion equation for each species in the liquid phase in and around the granule (Fick's diffusion is considered, as in most cases we are dealing with dilute, liquid-phase systems):

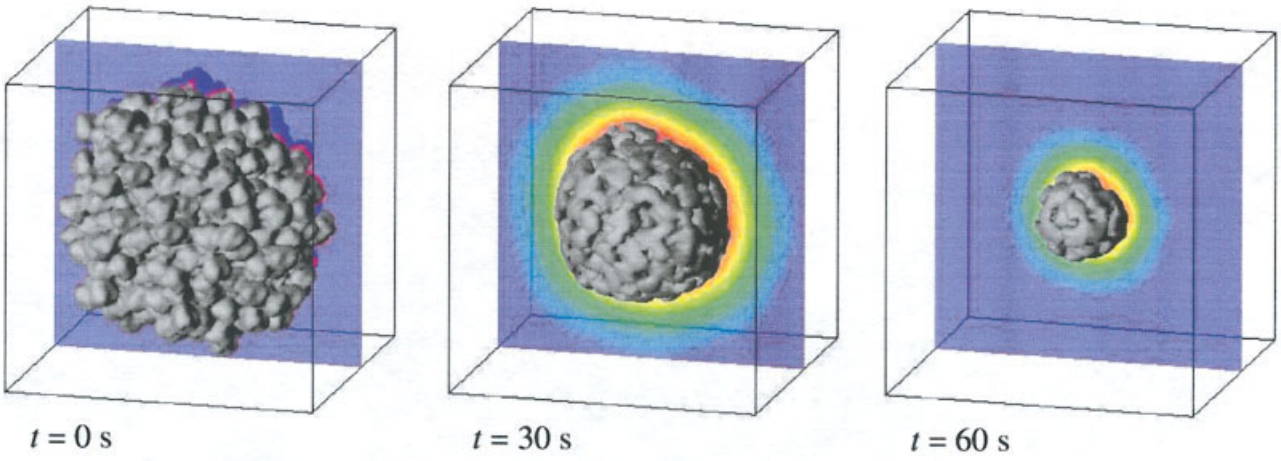

Figure 2. Illustration of the simulation of diffusion-limited dissolution of a virtual granule.

The solid-liquid interface is eroded according to the local diffusion mass flux, obtained by solving the diffusion equation in the boundary layer within the surrounding fluid. [Color figure can be viewed in the online issue, which is available at www.interscience.wiley.com.]

$$\frac{\partial c_k}{\partial t} = D_k \nabla^2 c_k \tag{6}$$

simultaneously with the evolution equation for the phase functions (moving boundary problem) on all internal and external solid-fluid interfaces:

$$u_k(\mathbf{r}) = \begin{cases} \frac{1}{\rho_k}(-D_k \nabla c_k)\cdot \mathbf{n}_S(\mathbf{r}) & \forall\, \mathbf{r} \in \partial S \\ 0 & \text{otherwise} \end{cases} \tag{7}$$

In Eq. 7, $u_k(\mathbf{r})$ is the erosion rate of component k in point $\mathbf{r}$, $\mathbf{n}_s$ is the solid-liquid interface normal vector, and ∂S denotes the solid-liquid interface. The evolution equations for the phase functions are related to the erosion rate by:

$$\frac{df_k(\mathbf{r})}{dt} = -\frac{1}{h} u_k(\mathbf{r}) \tag{8}$$

where h is the spatial discretization step. The boundary conditions for Eq. 6 are $c_k = c_k^* \; \forall \mathbf{r} \in \partial$S, and $c_k = c_k^{bulk}$ on the boundaries of the diffusion sub-layer of thickness δ_D (for dissolution in excess liquid, $c_k^{bulk} = 0$; otherwise c_k^{bulk} is coupled with the granule dissolution via mass balance). The thickness of the diffusion boundary layer is calculated from the Sherwood number $Sh \equiv L/\delta_D$, where the characteristic length-scale, L, is taken to be the equivalent-volume diameter of the granule (the granule volume is calculated as the minimum convex envelope of the solid phase). The Sherwood number is evaluated from the well-known correlation

$$Sh = 2.0 + 0.60\, Re^{1/2}\, Sc^{1/3} \tag{9}$$

where $Re \equiv UL/\nu$ and $Sc \equiv \nu/D$ are the Reynolds and the Schmidt number, respectively. It should be noted that Eq. 9 can only be applied if the diffusion sub-layer thickness is sufficiently larger ($\sim$10$\times$) than the surface asphericities of the granule; otherwise, the full convection-diffusion problem should be solved around the granule.[14] The dissolved fraction of each of the K components as a function of time is obtained by numerical integration of Eqs. 6 and 8, and from it the three dissolution times $[t_{10},t_{50},t_{90}]$. The evolution of a single-component granule with parameters $c^* = 0.252$ gcm^{-3}, $D = 0.905 \times 10^{-5}$ cm^{2}s^{-1}, and $\rho = 1.35$ gcm^{-3} (these values correspond to D-mannitol in water at 25°C) during dissolution at $Re = 1.6$ is shown in Figure 2 for illustration. The color-map surrounding the granule structure represents the concentration profile.

Granule Formation Model. The granule formation model has been fully described in our recent work,[15] and only the main principles will be repeated here. The modeling of granule formation from its constituent elements (primary solid particles and binder droplets) proceeds by random sequential deposition of the primary objects into a simulation unit cell where they are attracted to an imaginary center of gravity, positioned in the middle of the unit cell—see Figure 3. The asymptotic position of each incoming particle is found by the ballistic deposition algorithm.[16] In the absence of binder, a close random packing of primary solid particles is formed; in the model, the particles are allowed to overlap slightly (typically 1-5% of the particle volume) at the contact points. The shape, size distribution, and order of addition of the primary particles determine the structure of the virtual granule—its void fraction and the radial distribution of components. In this work, only binderless granules are considered. Detailed analysis of the effect of binder droplet spreading and solidification on granule microstructure can be found in reference[15].

Structure-Dissolution Relationships

Effect of primary particle size and radial distribution of components

Before addressing the full granule design problem for a specific system, let us investigate the relationship between granule structure and its dissolution rate for the simplest possible case: a model two-component system (solids S_1 and S_2) without binder. Primary particles in this case are partially fused—computationally this is achieved by allowing a small particle overlap during the close random packing. For a fixed

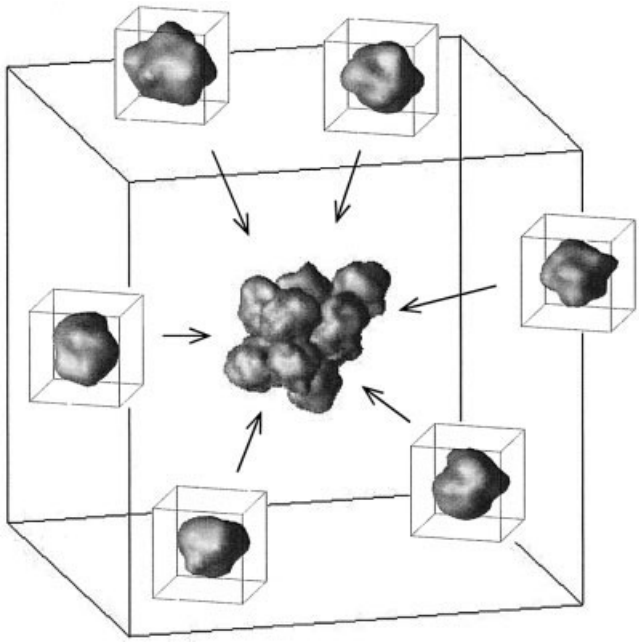

Figure 3. Illustration of the ballistic deposition method for the construction of virtual granules.

The primary particles are inserted into the simulation unit cell from random directions and attracted to an imaginary center of gravity in the middle of the box.

composition, the distribution of an active (be it S_2) within the granule can be varied in two modes, as illustrated in Figure 4. In cases a-c the particle size of the active is changing, but the distribution of the particles within the granule is random and spatially uniform—the structures are isotropic. On the other hand, in cases d-f the particle size remains the same but the radial distribution of the active within the granule is changing—the structures are layered.

Three-dimensional granule structures composed of a binary mixture of S_1 and S_2 particles have been generated by the method described in the section "Granule formation model." In the first series of structures, the composition was kept constant at 50% by volume of S_2. and the only variable parameters were primary particle size of S_2 and its distribution within the granule. The values of solubility, diffusion coefficient, and density were $c^* = 0.252$ gcm^{-3}, $D = 0.905 \times 10^{-5}$ cm^{2}s^{-1}, and $\rho = 1.35$ gcm^{-3}, respectively, for both components in order to investigate the pure effect of granule structure on dissolution. The default primary particle diameter was $d_p = 90$ μm with dimensionless surface roughness amplitude and correlation length (for definitions, please refer to reference [17]) of $a = 0.33$ and $L_c = 0.17$, respectively. Granules containing 500 primary particles have been generated; the equivalent diameter of the resulting granules was $d_g = 840$ μm and their porosity $\varepsilon = 0.28$ in all cases. The structures are shown in Figure 5a-f.

Case a is the default case—a random mixture of equal-size primary particles. Cases b and c have the same composition by volume as case a, that is 50% of S_2, but were realized from S_2 particles having a smaller ($d_p = 60$ μm) and larger ($d_p = 120$ μm) diameter than in the base case, respectively. The number of particles was adjusted in these cases in order to maintain the volume fraction of the S_2 component at 50%. In cases d, e, and f, the primary particle diameters are back to the default value but the order of addition of the S_1 and S_2 primary particles was varied. Granule in case d was formed by first adding 250 S_1 primary particles and then 250 S_2 particles (the active is in the shell). In case e, the order of addition was 50 S_1 followed by 250 S_2 and, finally, the remaining 200 S_1. Case f is similar to case d, only the roles of S_1 and S_2 have been switched (active in the core).

Dissolution simulations of granule structures from Figure 5a-f have then been carried out. Their results are summarized in Figures 6 and 7. It should be noted that the overall dissolution time of the granules was the same in all cases (regardless of structure) because the physico-chemical properties of the two solids were chosen to be identical and the total granule volume was also essentially the same in all cases. However, the release rates of the individual components were different due to their different spatial distribution within the structure. In Figure 6 the fraction of S_2 in the remaining undissolved granule is plotted as a function of elapsed time during dissolution. It, therefore, gives an indication of the qualitative and quantitative difference in the release dynamics of component S_2 in the various cases. In case a, the composition remains at 50% of S_2 throughout the dissolution due to the random dispersion of the S_2 component within the granule. The small deviation from the 50% baseline in the final stages of dissolution is simply due to the discrete nature of the granule—the few particles in the center happen to be slightly outnumbered in favor of S_2. Looking at case b we can see that when the particles of the S_2 component are smaller than in the default case, they tend to dissolve faster (presumably due to the larger specific surface area) and, consequently, the remaining granule has less than 50% of S_2. On the other hand, as the curve for case c shows, when the S_2 particles are comparatively larger, their dissolution rate is slower and the granule becomes enriched by that component (the curve c is above the 50% baseline).

Figure 6 further shows that the core-shell structures have an even stronger influence on the release profile of the active than particle size (compare the related problem of non-uniform catalyst distribution in heterogeneous catalyst pellets[18]). In case

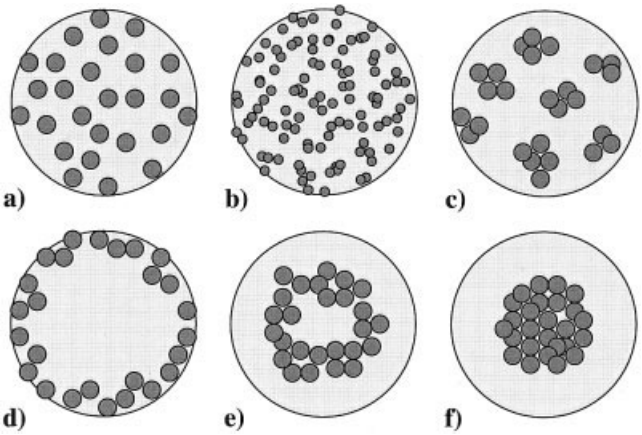

Figure 4. Possible distribution of an active ingredient within a granule.

Cases a-c show a random dispersion of normal, milled, and pre-agglomerated particles of the active. Cases d-f show the active located in the shell, in an intermediate layer, and in the core of the granule.

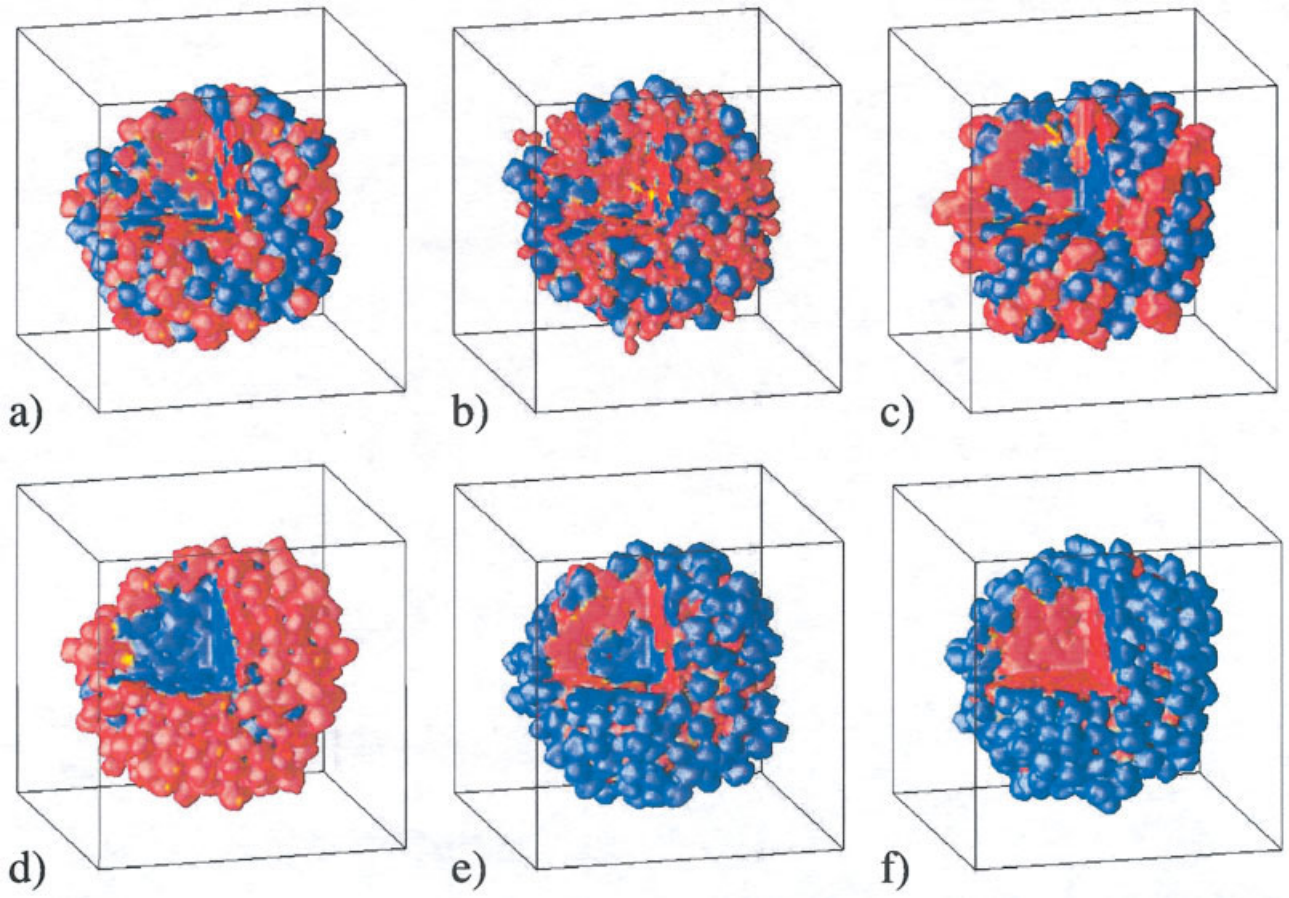

Figure 5. Virtual granules formed by the ballistic deposition algorithm and mimicking the model structures from Figure 4.

The composition of the granule is 50% of each of the two solid components on a volume basis. [Color figure can be viewed in the online issue, which is available at www.interscience.wiley.com.]

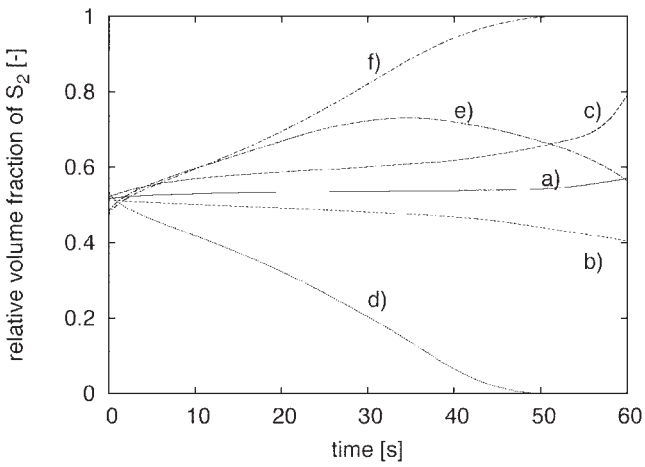

Figure 6. Relative volume fraction of component S_2 (the active) in a granule during dissolution.

The labels at the curves denote the corresponding structure from Figure 5. Curves below the 50% baseline mean that the active is preferentially released from the granule, and vice versa.

d when the S_2 component is in the shell, its release is rapid and its fraction in the remaining granule drops sharply. On the other hand—case f—when the active component is in the core, its

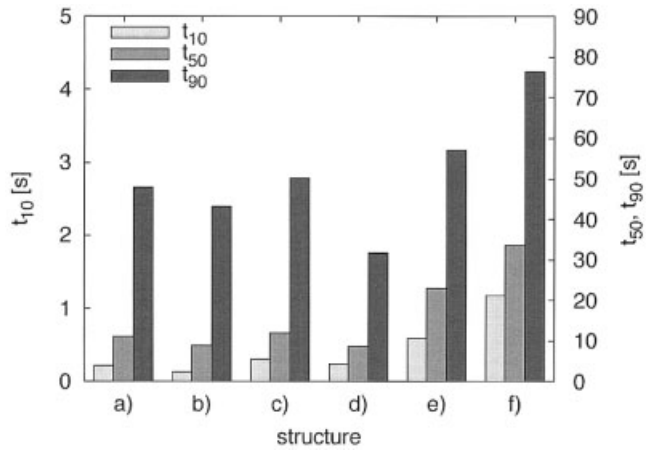

Figure 7. Integral characteristics (dissolution times t_{10}, t_{50}, and t_{90}) evaluated from the computational dissolution of structures shown in Figure 5.

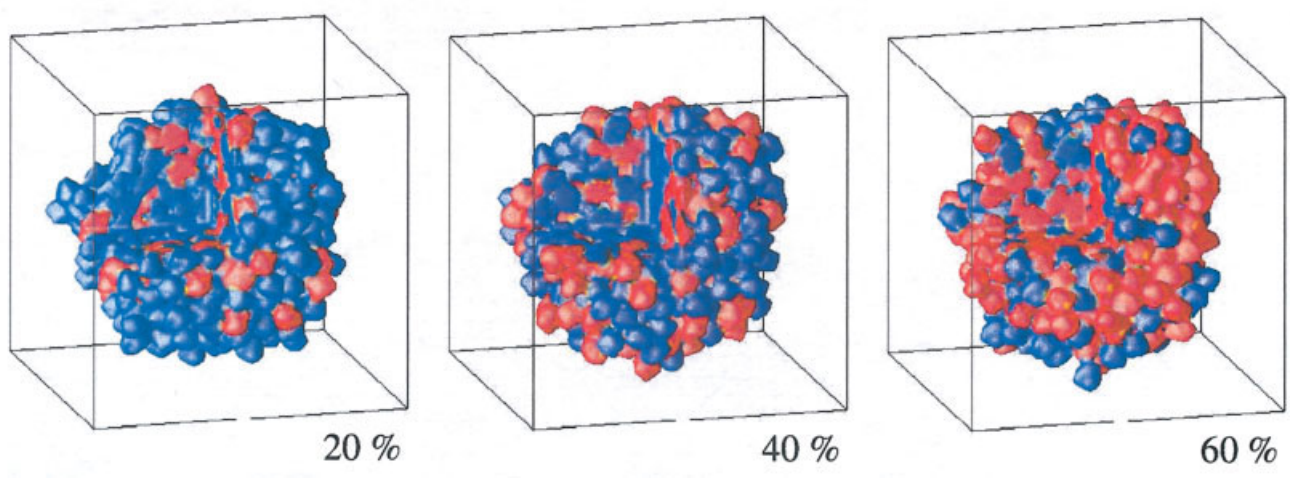

Figure 8. Binary granule with a varying composition of the active component.

The 20% case represents a structure where S_1 is above its percolation threshold and S_2 below; the 40% case is a characteristic bi-continuous structure (both components are above the percolation threshold); and the 60% case is a transition case where the S_1 component is just around its percolation threshold while S_2 percolates. [Color figure can be viewed in the online issue, which is available at www.interscience.wiley.com.]

release is delayed and the granule becomes rapidly enriched by S_2. The intermediate, layered case e shows a combination of the above trends, with a characteristic maximum clearly apparent on the residual composition curve. The integral characteristics, that is, the dissolution times t_{10}, t_{50}, and t_{90} for the S_2 component, and all six cases are plotted in Figure 7. This graph confirms the trends observed on the composition curves in Figure 6, that clearly the distribution of the active component within the granule has a strong effect on the release profile. The core-shell structures in particular seem to be very effective in controlling the release times—the t_{90} is more than twice in case f (S_2 in core) than in case d (S_2 in shell).

Effect of composition

In the above study, the net effect of component distribution within a granule structure on its release rate was shown. The computational study made it possible to keep the physicochemical properties of both components exactly the same. Let us now investigate the effect of non-equal individual dissolution rates (due to a difference in the component properties: solubility, density, or diffusion coefficient) on the release rate of the active ingredient from a granule structure. In this case the structure itself will be kept simple—the default case of a random mixture of two components with equal particle size and shape will be considered (case a from Figure 5). The properties of S_1 will be kept at the default values; however, those of the S_2 component will be set to $c^* = 0.359$ gcm^{-3}, $D = 1.99 \times 10^{-5}$ cm^{2}s^{-1}, and $\rho = 2.17$ gcm^{-3} (corresponding approximately to NaCl in water at 25°C).

Granules consisting of 500 primary particles (equivalent granule diameter $d_g = 840$ μm, porosity $\varepsilon = 0.28$) were generated with varying volume fraction of randomly distributed S_2 particles, ranging from 0 to 1 in 0.1 increments. Three such structures are shown in Figure 8 for illustration. They represent cases of S_2 below the percolation threshold, bi-continuous structure, and S_1 below its percolation threshold. The dissolution time t_{90} of components S_1 and S_2 and of the entire granule, as a function of composition, is plotted in Figure 9. The figure shows that the pure-component dissolution times are indeed different in this case due to their different physicochemical properties. It also shows that the dissolution of each component is the fastest (limiting case is $t_{90} \rightarrow 0$s) when that component is dilute within a granule composed almost entirely of the other component. Due to the relatively high granule porosity in this case ($\varepsilon = 0.28$, percolating voidage), all primary particles are in contact with the liquid phase at all times. When a given component dominates the structure, the liquid in the pore space of the granule becomes saturated relatively quickly and only primary particles on the outside of the granule can dissolve thanks to the external diffusion in the boundary layer. However, isolated particles of a given component within the structure can dissolve effectively as if they were isolated in the liquid and, therefore, their dissolution is very fast.

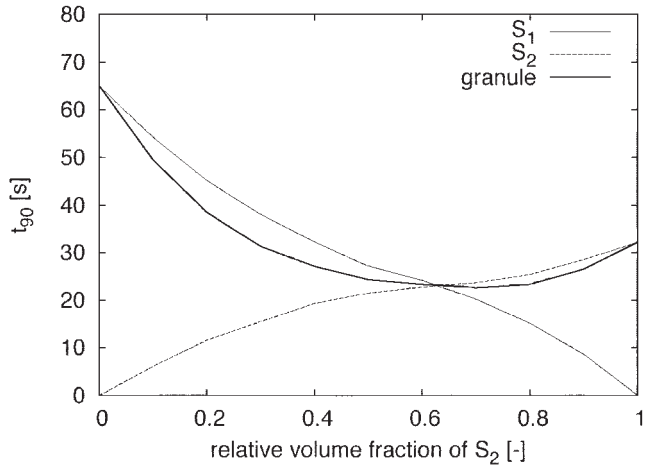

Figure 9. Dependence of the dissolution time t_{90} on granule composition for a granule with porosity of 28%.

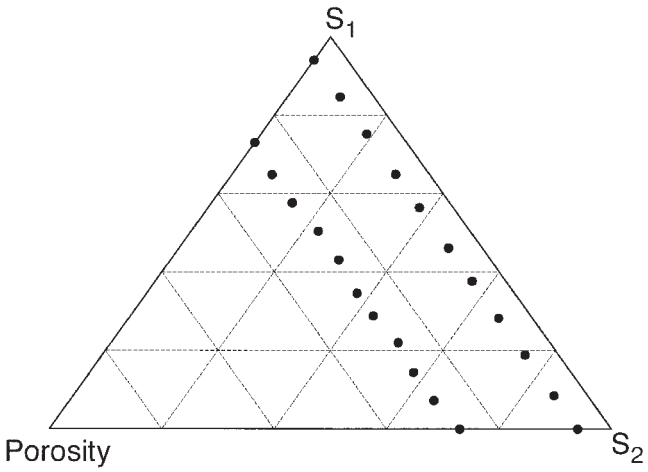

Figure 10. Triangular diagram showing the compositions of granules used in the dissolution study.

Two granules' porosities—6 and 28%—have been realized, and for each porosity the relative volume fraction of the S_2 component was varied from 0 to 1 in 0.1 increments.

The combination of the monotonously increasing t_{90} for S_2 as a function of its volume fraction in the granule, and the monotonously decreasing t_{90} for S_1 gives rise to a minimum in the overall dissolution time for the entire granule, as is apparent in Figure 9. The existence of this minimum is very interesting as it means that, although S_2 is the faster-dissolving component of the two, a granule composed entirely of it is not necessarily the fastest-dissolving granule. An even faster dissolution (t_{90} = 22 s at the optimum point as opposed to 32 s for the S_2-only granule) can be achieved by diluting the S_2 particles in the granule by another component (S_1), even if this component on its own is slower-dissolving than S_2 (t_{90} = 65 s for S_1-only granules). This finding is very significant for product formulation.

The case discussed above was characteristic by the fact that all primary particles within the granule structure were in direct contact with the liquid phase and had a diffusion path to the granule surface at all times during dissolution thanks to the relatively high porosity. The composition of a two-component porous granule can be represented by a point in the triangular phase diagram, as shown in Figure 10. Each dot in the figure represents a single granule that was realized and its dissolution modeled. In the second series of computational experiments, the fraction of S_2 in the granule was again varied from 0 to 1 but the porosity was lower at approximately $\varepsilon = 0.06$. This was achieved by allowing a larger (0.25) inter-particle overlap in the packing algorithm. The primary particle size and shape were kept the same as in the previous (large porosity) case; hence, the number of primary particles required to form the granule had to be increased in order to maintain the same granule diameter (d_g = 840 μm). The physico-chemical parameters of components S_1 and S_2 were also kept the same as in the low-porosity case.

The dissolution time t_{90} as a function of the S_2 fraction in the granule for the low-porosity case is plotted in Figure 11. Three features are immediately noticeable. First, the granule dissolution time is longer in this case due to the lower porosity (larger volume fraction of solids in a granule of identical size). Second, the granule dissolution time again has a minimum as a function of composition, and the position of this minimum is relatively close to that in the high-porosity case (70% and 62% of S_2, respectively). This would suggest that high granule porosity is not a necessary condition for the existence of the minimum. Third—and this is the main qualitative difference from the high-porosity case—also the individual component dissolution times have minima with respect to composition, rather than being a monotonously increasing (S_2) or decreasing (S_1) function of the S_2 fraction in the granule. The reason for this behavior is that the 6% porosity is non-percolating and, therefore, the dominant component always blocks the dispersed one. This means that in the limit of $S_2 \rightarrow 0$ and $S_2 \rightarrow 1$ the dissolution times of both components are equal; for example, in the case $S_2 \rightarrow 0$, although in the high-porosity case the few dispersed particles in the granule structure could dissolve almost instantly, now they are blocked by the slower-dissolving S_1 phase surrounding them. Further analysis of the effect of percolation on the dissolution of multi-component tablets can be found in references [19-21]. It should also be noted that in the case discussed above, the two components did not influence each other's solubility of diffusion coefficient; in situations such as dissolution or surfactants or polymers in the presence of electrolytes, this is not the case and more complicated behavior can be observed.

In summary, the simulations performed in this section have provided the following design guidelines for granule structuring: (1) smaller primary particle size of the active generally leads to faster release rate; (2) core-shell structure is a very effective means of achieving delayed or phased release of the active, whereas random dispersion of the active within the granule leads to a gradual release; (3) the release rate of an active can be increased by forming a composite granule, even if the other ingredient(s) are individually dissolving at a slower rate than the active. In the following section, the design guidelines will be used for the physical preparation of granule batches with varying microstructure, and thereby experimentally confirmed (or otherwise).

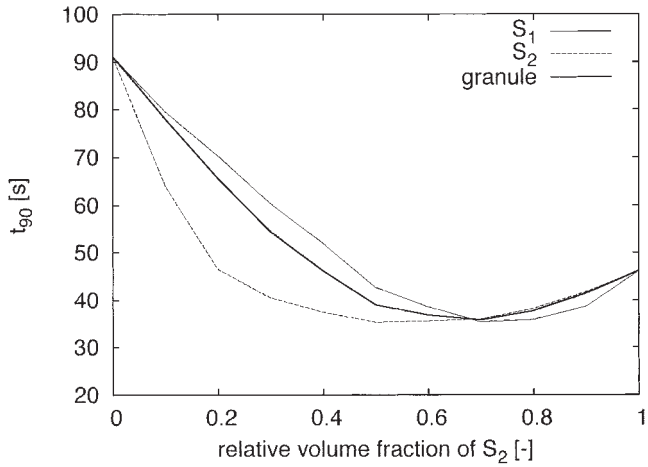

Figure 11. Dependence of the dissolution time t_{90} on granule composition for a granule with porosity of 6%.

Table 1. Summary of Granulation Process Conditions Used for the Preparation of Individual Batches

Batch	Process Mode	Primary Solids (S)	Binder (B)	B-S Ratio	NaCl to S Ratio	NaCl Size Range (μm)	NaCl Addition Mode
SPG-07	in-situ melt	Suglets	PEG	0.11	0.06	75–212	Dispersed within PEG binder
SPG-08	in-situ melt	Suglets	PEG	0.11	0.06	75–212	As dry particles mixed with Suglets
SPG-09	in-situ melt	Suglets	PEG	0.11	0.06	250–355	Dispersed within PEG binder
SPG-11	in-situ melt	Suglets	PEG	0.11	0.03	<32	Dispersed within PEG binder
MHC-01	spray	Mannitol	Aqueous HPC	0.02	0.05	75–212	As dry particles mixed with Mannitol
MHC-02	spray	Mannitol	Aqueous HPC	0.02	0.02	N/A	As aqueous solution with HPC binder

Experimental Realization

Materials

Granules for this study were prepared by fluid-bed granulation from sugar spheres "Suglets" (NP Pharm, France) and D-mannitol "Pearlitol-200SD" (Roquette, France) using polyethylene glycol (PEG) and aqueous solution of hydroxypropyl cellulose (HPC) as binders, respectively. The two solids are common pharmaceutical excipients, and the binders are typical examples of a melt and aqueous binder, respectively. The sugar spheres are themselves agglomerates composed of sucrose (92% dry basis) and maize starch. They offer good control in granulation due to their high sphericity and narrow particle size distribution. The particle size range of Suglets used in this study was 250-355 μm. The PEG binder (mol. wt. 6000; VWR, UK) used for melt granulation of the Suglet particles was milled and sieved; the 710-1000 μm size fraction was used in granulation. The mannitol used was a spray-dried powder; the 150-250 μm size fraction was used for granulation. With mannitol, a 5% aqueous solution of HPC (Fisher Scientific, UK) was utilized as a spray-on liquid binder. Sodium chloride (Fisher Scientific, UK) was used as a model water-soluble active ingredient in granule formulation. The active ingredient (NaCl) was added as solid particles in the primary powder batch, as aqueous solution with the HPC binder, or as solid dispersion in the PEG binder depending on the required distribution of NaCl in the granule structure. The solid dispersion was prepared by introducing a specific amount of NaCl particles into molten PEG and then allowing the suspension to cool at ambient temperature under constant agitation. The agitation, which was necessary to keep uniform distribution of NaCl particles in the PEG continuum, was stopped when the suspension turned into paste. The paste was then left overnight to fully solidify, and finally milled and sieved.

Granulation protocol

Granulation for both systems (NaCl-Suglets-PEG and NaCl-mannitol-HPC) was performed in a desktop fluidized bed granulator of the 4M8 range (Pro-C-epT, Belgium) equipped with computer logging of process parameters. PEG was applied as in-situ melt binder, while HPC was added as aqueous solution through a top spray. A single melt granulation experiment consisted of three steps: mixing, heating, and cooling. A 200 g batch composed of Suglets and PEG particles, together with NaCl in the appropriate form, was first fluidized at ambient temperature for approximately 120 s to achieve mixing. The inlet air flow-rate was kept in the range of 1.4-1.5 m^3/min. Temperature of the bed was then raised at the rate of 7-10°C per minute to 60-65°C (that is, just above the melting point of the PEG binder) and maintained at the same level for 120 s. Agglomeration occurred in this stage. Finally, the bed was gradually cooled down to 40°C before discharging.

The spray granulation procedure used for the mannitol-HPC system may also be divided into three steps, namely: heating, agglomeration, and drying. A mass of 200 g of mannitol or mannitol and NaCl was fluidized by maintaining the air flow-rate in the range of 0.5-0.6 m^3/min (due to smaller particle size and density compared with Suglets). Temperature of the bed was raised to 50°C before introducing 70 ml of the aqueous solution of HPC or HPC and NaCl as a top spray through a two-fluid nozzle at a flow-rate of 15 ml/min. The solution was sprayed in two intervals, that is, the spray was stopped for 60 s after the addition of 25 ml and then for 120 s after dosing further 25 ml. These time intervals were necessary to keep the bed in a fluidized state. The nozzle height and atomizing air pressure were kept constant throughout the study. The addition of aqueous binder caused the process temperature to drop—the bed had a temperature of approximately 40°C during the binder addition phase. The drying regime was started immediately after completing the dosage of the liquid binder, and the granulation end-point was taken when the bed again reached ~50°C (the inlet air temperature). Table 1 provides a summary of the batches prepared using the above-mentioned protocols. SEM images of typical Suglet- and mannitol-based granules are shown in Figure 12. The Suglet-based granules are visibly rounder and more compact, due to the in-situ melt granulation technique (immersion mechanism[22,23]).

Structure analysis

Granule microstructure was characterized by means of X-ray micro-tomography[24] using the SkyScan 1072 desktop X-ray micro-tomograph (SkyScan, Belgium). Granule samples were scanned using a 0.9° scan step from 0 to 180°, and the typical acquisition time was around 25 min. Cross-sectional pixel size in the range of 3.66-4.20 μm was maintained for all samples. Cross-sectional and three-dimensional images were reconstructed using the SkyScan software package. Both transmission and reconstructed X-ray images of selected granules can be seen in Figure 13. The gray-scale level in the image is proportional to the local X-ray attenuation in the granule structure, which in turn is proportional to the density. Hence, the NaCl, Suglet primary solid particles, and pore-space can be clearly distinguished. Segmentation of the PEG binder, on the other hand, would require the use of specialized segmentation algorithms.[25]

Dissolution rate measurement

Dissolution tests were carried out in duplicate in a 400 ml beaker filled with 250 ml of de-ionized water at a constant

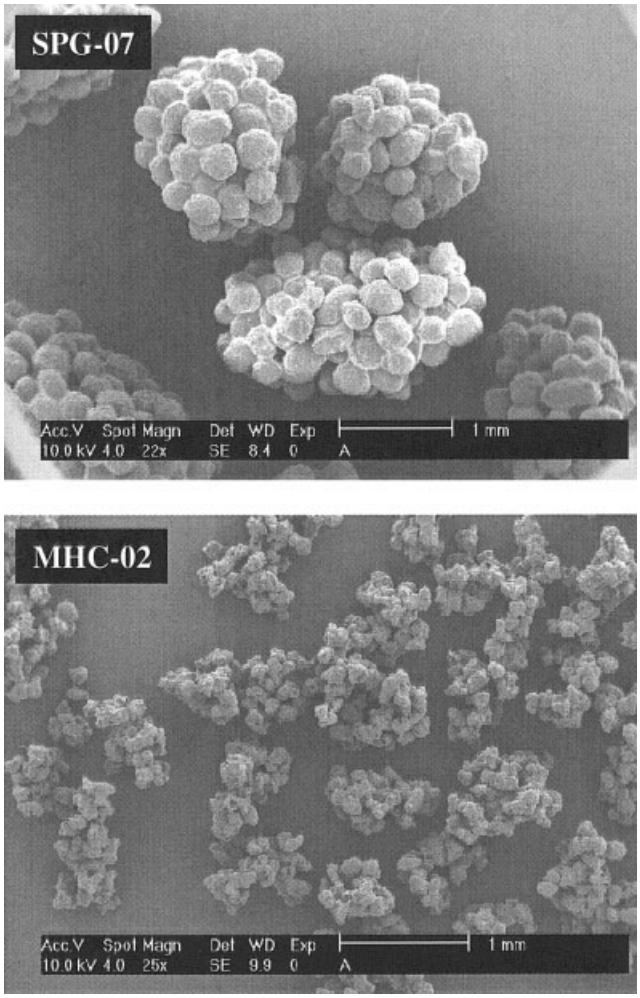

Figure 12. SEM micrographs of granule samples from batches SPG-07 (NaCl-Suglet-PEG as in-situ melt binder) and MHC-02 (NaCl-mannitol-HPC as spray-on aqueous binder) .

For details of granulation conditions, please refer to Table 1.

temperature of 20°C. A granule sample of 1.00 g was introduced, and the release of NaCl in water was monitored by measuring conductance (Jenway, model 4510) of the dissolution medium at constant time intervals. The batch was stirred by an overhead stirrer at 50 rpm. The height and speed of the stirrer were chosen so that the sample granules were not in direct contact with the stirrer blades in order to avoid mechanical attrition and breakage. As a result, granule disintegration did not occur in any of the cases discussed below (that is, the granules dissolved predominantly by the shrinking-core mechanism). The selected size ranges for dissolution study were 1000-1500 μm for Suglet-based and 500-710 μm for mannitol-based granules. As a reference, the intrinsic dissolution of NaCl particles was also measured. The particles were introduced into the system as 20% by weight suspension in iso-propanol (VWR, UK) to keep the individual particles physically separated. If introduced directly, the particles had a tendency to form aggregates and affect the dissolution rate. Iso-propanol has been chosen as the dispersion aid because it is an anti-solvent for NaCl but at the same time it mixes well with water. The total quantity of iso-propanol introduced into the system was small enough (0.5 ml) not to affect the dissolution of NaCl in water.

Results and Discussion

Granule structures

Batches of granules containing NaCl as a model "active" and consisting of Suglet and mannitol primary particles with PEG and aqueous HPC binder, respectively, were prepared according to the protocol described above and summarized in Table 1. The X-ray shadow images of granules randomly selected from batches SPG-07, SPG-08, SPG-09, and SPG-11 and their corresponding reconstructed mid cross-sections are presented in Figure 13. These images clearly show a strong influence of the method of addition of the active on granule microstructure. The NaCl crystals appear in the X-ray images as dark pixels due to their higher density (hence, X-ray attenuation coefficient), and are easily distinguishable within the light-gray structure of the granule.

In our recent work[23] it was shown that in in-situ melt granulation, when the binder particle size was relatively coarser than the primary solids, the particle build-up process follows the immersion and layering mechanism and hollow-core granules are formed. According to this mechanism, a binder particle serves as a nucleus for a single granule and the growth occurs by a gradual build-up of primary solids on the surface of the nucleus. As the binder particle melts, the liquid is drawn by capillary forces into the upper granular structure and thus develops a hollow core. Granule batches SPG-07, SPG-09, and SPG-11 were prepared using this approach.

For batch SPG-08, which was prepared by granulation of a mixture of NaCl and Suglet particles, it can be seen that the spatial distribution of NaCl within the granule structure was random. The images of batch SPG-11 also show the spread of fine NaCl particles throughout the granule, but in this case they generally positioned themselves between the co-ordination points of the primary solids, along with the PEG binder. On the contrary, the active ingredient in the granules belonging to batches SPG-07 and SPG-09 restricted itself to the middle section as core, and these structures may therefore be called encapsulated granules. The main factor affecting the spatial distribution of NaCl crystals in cases SPG-07, SPG-09, and SPG-11 was their size. When the size of NaCl crystals, in solid solution with PEG, was less than 32 μm (batch B), it was uniformly transported by molten binder through the inter particle pores to all over the structure. On the other hand, the advancement of the NaCl particles seems to be limited within the core section when its size in solid solution was comparable with primary solids (batch SPG-07 and SPG-09, respectively). Batch SPG-09 granules represent the case where the active (size range 250-355 μm) did not flow with the binder along the pores at all. Thus, the method of addition of actives or any other component as solid dispersion in a melt binder represents an effective way to control its positioning within the granule matrix, and in this novel technique the ratio of active-ingredient particle size to primary solids appears to be an important variable.

The effect of different means of addition of NaCl on granule microstructure was also studied for the mannitol-HPC system using the conventional spray-granulation mode. Two batches

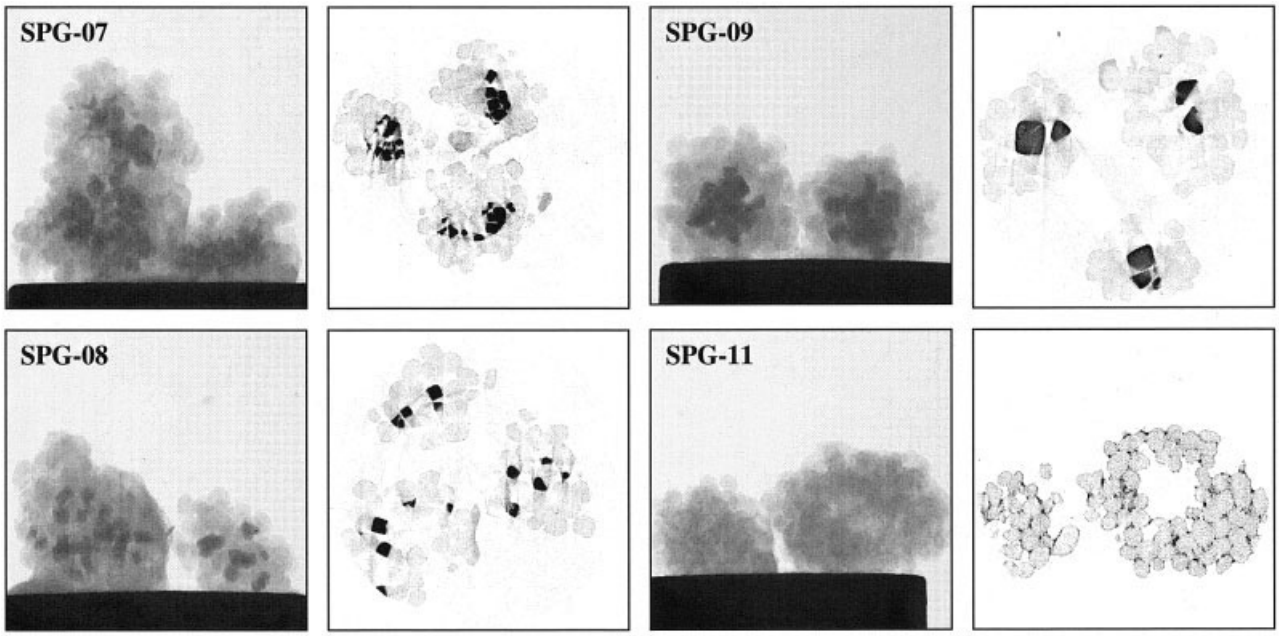

Figure 13. X-ray micro-tomography images of NaCl-Suglet-PEG granules (please refer to Table 1 for details of granulation conditions) .

In each case, the left column shows a transmission image and the right column a horizontal cross-section of the granule after beam reconstruction. The dark areas are NaCl particles.

were prepared, namely, batches MHC-01 and MHC-02 (see Table 1). In the preparation of the former, NaCl was introduced as particles with primary solids, while in the latter case NaCl was added as 5% secondary solute into the HPC solution. The tomographic images of granules from these batches are not shown. Batch MHC-01 bears a qualitative similarity with the corresponding melt binder case (batch SPG-08) in that the granules contain randomly distributed NaCl crystals within the structure. In contrast, batch MHC-02 granules can be considered as a limiting case for the NaCl particle size tending to zero, and the structure therefore bears a qualitative similarity to SPG-11. The NaCl component coincides with the HPC binder at the mannitol particle contact points.

Dissolution profiles

Figure 14 shows the dissolution curves of granules from batches SPG-07, SPG-08, SPG-09, and SPG-11, and the intrinsic dissolution of NaCl particles, which were in the size range of 75-212 μm. As shown in the figure, despite constant binder-to-solid ratio of 0.11 that was maintained in all the cases, dissolution profiles especially in the initial phase are significantly different. Notice the initial time lag in release, which is considerable for the cases SPG-07 and SPG-09, that is, those where NaCl is located in the core. On the other hand, NaCl release is more gradual in the two cases where NaCl particles are randomly distributed within the granule (SPG-08 and SPG-11). Notice, however, that in case SPG-11, although the NaCl particles are smaller than in case SPG-08, the dissolution rate is slower due to the fact that the salt particles are immersed in the PEG binder. This situation is similar to the high- and low-porosity cases discussed in the computational section: in case SPG-08 the salt particles have immediate access to the liquid phase, whereas in case SPG-11 their dissolution is hindered by the slower-dissolving PEG.

The release behavior exhibited by granules SPG-07 was also very interesting, although not totally unexpected. As can be seen in the tomographic images (Figure 13), NaCl particles formed a core inside the granule and, hence, were completely surrounded by the Suglet particles and the binder. This structural setting provides virtually no contact between the NaCl particles and the dissolution medium, and this is also perceptible by the dissolution behavior. It is shown in the graph that for about 160 s, there is practically no release of NaCl, con-

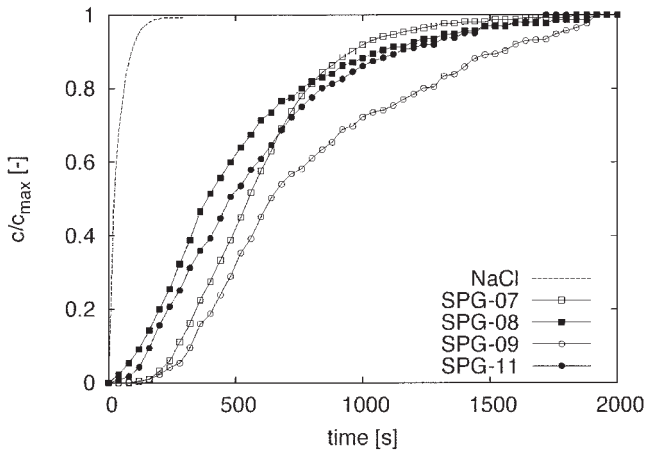

Figure 14. Experimental dissolution curves of NaCl-Suglet-PEG granules and of pure NaCl.

On the y-axis is the relative concentration of NaCl in the solution.

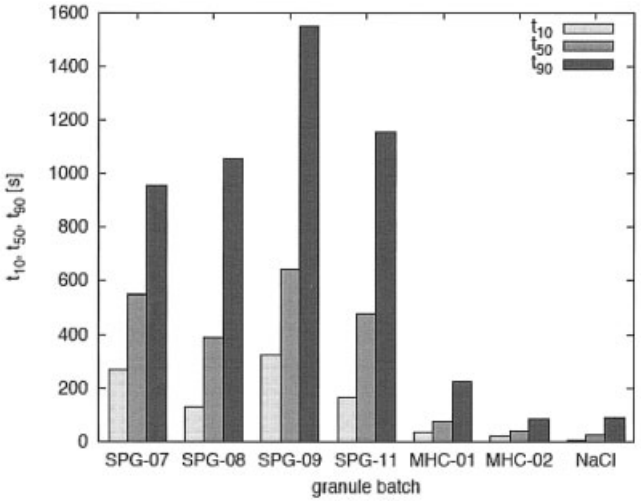

Figure 15. Dissolution times t_{10}, t_{50}, and t_{90} for the model active (NaCl) released from granules prepared as specified in Table 1 (the full dissolution curves can be seen in Figures 14 and 15).

firming the argument that the shell needs to be dissolved first before reaching to the active core by the dissolution medium. But once the medium reaches to the core, the dissolution rate was much faster and the release curve even slightly exceeded that of case SPG-08. This is nicely demonstrated by comparing the t_{10}, t_{50}, and t_{90} times plotted in Figure 15: while SPG-07 has longer both t_{10} and t_{50}, its t_{90} is comparable to that of SPG-08.

The other trend predicted in the computational section, that is, that the smaller the particles, the faster the dissolution under otherwise identical conditions, was validated next. Batch SPG-09 was prepared with larger NaCl particles (250-355 μm). As far as the initial time delay phenomenon is concerned, this batch exhibited more or less similar behavior as was noted in batch SPG-07 (see the t_{10} times in Figure 15); however, in this case the subsequent release was somewhat slower, also evident by the large value of t_{90} (1550 s).

The effect of the method of active ingredient addition on the dissolution of granules produced by spray granulation is illustrated in Figure 16. The time scale in this case is much shorter because of the open structure and smaller granules (see Figure 12). However, apart from the time scale, the shape of curve MHC-01 in Figure 16 is very similar to the corresponding curve SPG-08 in Figure 14—that is, both batches were prepared from a dry mix of NaCl and excipient particles and, therefore, contain a structure with randomly distributed NaCl particles. On the other hand, when NaCl was added as aqueous solution in granule formulation (batch MHC-02), the release was instant and comparable with the intrinsic dissolution rate of isolated NaCl crystals in the size range of 75-212 μm. This is probably because of the formation of a submicron layer of NaCl, which provides large surface area and, hence, greater contact to the dissolution medium.

In summary, it can be said that all three main qualitative trends predicted by simulations in the section "Structure-dissolution relationships" have been observed in experimental structures: (1) smaller particles size means faster dissolution; (2) core-shell structures cause an initial time lag in release; and (3) in situations where the active particles are completely surrounded by a non-porous matrix of another formulation component (the PEG binder in this case), their dissolution rate is fundamentally limited by that of the matrix component.

Conclusions

In this work the problem of granule microstructure design was formulated in mathematical terms. Two approaches for the solution of the design problem have been proposed—the stochastic design approach, which is based on random permutation of points within the granule structure, and the variational approach, which is based on computer simulation of granule structure formation and dissolution. A parametric study of the effect of particle size, radial distribution of components within the granule, and the granule composition and porosity on the release rate of the active has been performed and used to generate basic design guidelines for granule microstructure. These guidelines were then used for the physical preparation of granule batches with varying internal structure. The predicted effects of primary particle size on dissolution rate, as well as the effect of core-shell versus random distribution of the active within the granule, have been confirmed experimentally. The predicted maximum of release rate as a function of granule composition is still to be confirmed in future experiments.

A novel approach to controlling the spatial distribution of the active ingredient (or any other component, for that matter) within the granule structure, by employing the in-situ melt granulation technique, has been demonstrated. The arrangement of the active ingredient in the composite matrix was shown to have a profound influence on the dissolution profile. When the component of interest is randomly distributed, the release was found relatively faster and without any initial time lag. The initial time delay in release was observed when the active ingredient was encapsulated by the excipient particles, and its subsequent dissolution response was found dependent on the particle size of the active component.

The method of addition of the active ingredient also plays an important role in the granules prepared by the spray granulation

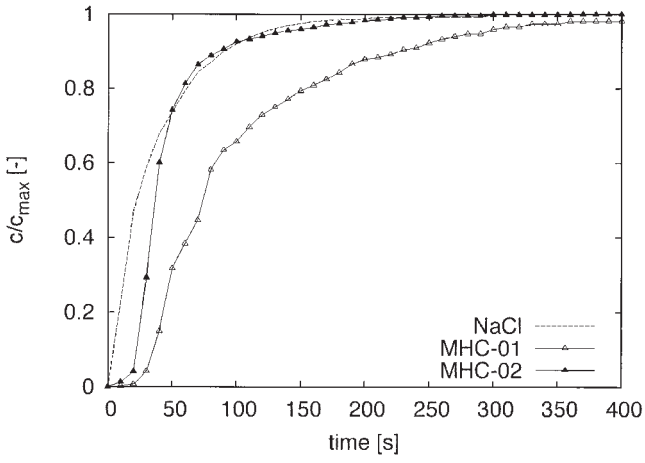

Figure 16. Experimental dissolution curves of NaCl-mannitol-HPC granules and of pure NaCl.

On the y-axis is the relative concentration of NaCl in the solution.

mode. In the case when the active component was randomly dispersed, the shape of the dissolution curve, although with much shorter time scales, was found similar to the corresponding batch prepared by the in-situ melt binder. When the active ingredient was added as aqueous solution together with the binder in the granule formulation, the release was found instant and comparable with the intrinsic dissolution of the active component.

Acknowledgments

Financial support from the UK Engineering and Physical Sciences Research Council (grant no. GR/S69146/01) is gratefully acknowledged. We thank Dr. Judith Bonsall from Unilever R&D Port Sunlight for the kind availability of XRCT and SEM imaging facilities.

Notation

c = solute concentration, kgm^{-3}
d = diameter, m
D = diffusion coefficient, m^2s^{-1}
$D(f_k)$ = dissolution mapping
f = phase function
$\mathbf{g}$ = gradient of objective function
$G(\mathbf{x})$ = granulation mapping
h = spatial discretization step, m
K = number of formulation components
L = characteristic length, m
$\mathbf{n}$ = normal vector
N = grid size
o = objective function
p = probability
$\mathbf{r}$ = spatial coordinate
R = radius, m
Re = Reynolds number
Sc = Schmidt number
Sh = Sherwood number
t = time, s
T = temperature in simulated annealing
u = solid-liquid interface velocity, ms^{-1}
U = characteristic velocity, ms^{-1}
w = mass fraction
$\mathbf{x}$ = vector of granulation process parameters

Greek letters

δ_D = diffusion boundary layer thickness, m
ε = porosity
ν = kinematic viscosity, m^2s^{-1}
Ω = set of microstructures
ρ = density, kgm^{-3}

Subscripts and superscripts

10, 50, 90 = dissolution of 10%, 50%, and 90% of active
F = feasible
g = granule
H = hypothetical
k = formulation component
p = particle
s = solid

Literature Cited

1. Edwards MF, Instone T. Particulate products—their manufacture and use. *Powder Tech.* 2001;119:9-13.
2. Knight PC. Structuring agglomerated products for improved performance. *Powder Tech.* 2001;119:14-25.
3. Ansari MA, Stepanek F. The effect of granule microstructure on dissolution rate. *Powder Tech.* 2006; accepted.
4. Hill M. Product and process design for structured products. *AIChE J.* 2004;50:1656-1661.
5. Fung KY, Ng KM. Product-centered processing: pharmaceutical tablets and capsules. *AIChE J.* 2003;49:1193-1215.
6. Lukas G. Critical manufacturing parameters influencing dissolution. *Drug Info J.* 1996;30:1091-1104.
7. Kosek J, Stepanek F, Marek M. Modeling of transport and transformation processes in porous and multiphase bodies. *Adv Chem Eng.* 2005;30:137-203.
8. Metropolis N, Rosenbluth AW, Rosenbluth MN, Teller AH, Teller E. Equations of state calculations by fast computing machines. *J Chem Phys.* 1953;21:1087-1092.
9. Stepanek F. Stochastic design of granule microstructure. *Comp Chem Eng.* 2006; submitted.
10. Yeong CLY, Torquato S. Reconstructing random media. *Phys Rev E.* 1998;57:495-506.
11. Torquato S, Hyun S, Donev A. Optimal design of manufacturable three-dimensional composites with multifunctional characteristics. *J Appl Phys.* 2003;94:5748-5755.
12. Torquato S, Hyun S, Donev A. Multifunctional composites: optimizing microstructures for simultaneous transport of heat and electricity. *Phys Rev Lett.* 2002;89:266601.
13. Edgar TF, Himmelblau DM. *Optimization of Chemical Processes*. New York: McGraw-Hill; 2001.
14. Stepanek F. Computer-aided product design: granule dissolution. *Chem Eng Res Design.* 2004;82:1458-1466.
15. Stepanek F, Ansari MA. Computer simulation of granule microstructure formation. *Chem Eng Sci.* 2005;60:4019-4029.
16. Coelho D, Thovert JF, Adler PM. Geometrical and transport properties of random packings of spheres and aspherical particles. *Phys Rev E.* 1997;55:1959-1978.
17. Stepanek F, Rajniak P. Droplet morphologies on particles with macroscopic surface roughness. *Langmuir.* 2006;22:917-923.
18. Morbidelli M, Gavriilidis A, Varma A. *Catalyst Design: Optimal Distribution of Catalyst in Pellets, Reactors, and Membranes*. Cambridge: Cambridge University Press; 2001.
19. Holman LE, Leuenberger H. The effect of varying the composition of binary powder mixtures and compacts on their properties: a percolation phenomenon. *Powder Tech.* 1990;60:249-258.
20. Luginbühl R, Leuenberger H. Use of percolation theory to interpret water uptake, disintegration time and intrinsic dissolution rate of tablets consisting of binary mixtures. *Pharmaceutica Acta Helvetica.* 1994;69:127-134.
21. Stepanek F, Loo A, Lim TS. Multiscale modeling methodology for virtual prototyping of effervescent tablets. *J Pharmaceutical Sci.* 2006; 95:1614-1625.
22. Schæfer T, Mathiesen C. Melt pelletization in a high shear mixer: IX. Effects of binder particle size. *Int J Pharmaceutics.* 1996;139:139-148.
23. Ansari MA, Stepanek F. Formation of hollow core granules by fluid bed in-situ melt granulation: modelling and experiments. *Int J Pharmaceutics*. 2006;321:108-116.
24. Farber L, Tardos G, Michaels JN. Use of X-ray tomography to study the porosity and morphology of granules. *Powder Tech.* 2003;132:57-63.
25. Kohout M, Grof Z, Stepanek F. Pore-scale modelling and tomographic visualisation of drying in granular media. *J Coll Interface Sci.* 2006; 299:342-351.

Manuscript received Apr. 20, 2006, and revision received July 17, 2006.